Engineering Geology 284 (2021) 106036

Contents lists available at ScienceDirect

Engineering Geology

journal homepage: www.elsevier.com/locate/enggeo

Smectites: The key to the cost overruns in the construction of the third set of locks of the Panama Canal

Mercedes Suárez [a,*], Emilia García-Romero [b], Ascensión Baz [c], Rafael Pérez [c]

[a] Department of Geology, University of Salamanca, 37008 Salamanca, Spain
[b] Department of Mineralogy and Petrology and IGEO, Complutense University of Madrid, 28040 Madrid, Spain
[c] SACYR Construcción, Madrid, Spain

ARTICLE INFO

Keywords:
Smectite
Basalt
Aggregates
Rapid degradation
Texture
Swelling clays
Accelerated aging

ABSTRACT

The third set of locks of the Panama Canal is one the most impressive civil infrastructures in the world. Its construction, however, was delayed by two years incurring cost overruns in billions that were mainly related to the use of the local basalt as the raw material for concrete production. The rapid degradation during the construction of an apparent sound basalt resulted in the huge loss of fines during the manufacturing of concrete. In the rock, olivine and glass are, respectively, altered to iddingsite and palagonite that are mainly composed of smectites. Smectites are also found around plagioclase and pyroxene crystals and filling the dense network of micro- and nano-cracks. Moreover, these smectites are spatially interconnected, which is the key to explaining the unexpected behavior and the rapid degradation of the basalt. Such a rapid degradation of basic igneous rocks – exposed to the weather and then utilized as a construction material – is not frequent, yet it is significant enough to call for the development of a new standard for the use of these materials in construction.

1. Introduction

The third set of locks of the Panama Canal (Fig. 1a, b), one the most impressive civil infrastructures in the world, was inaugurated in 2016, two years after the scheduled date. The delay in the construction and the millionaire cost overruns incurred were mainly attributable to the use of local basalt as the raw material for concrete. The construction required an excavation of ~50 · 10^6 m^3 of rock and over 5 · 10^6 m^3 of concrete for which aggregates and sands derived from the crushing of local basalt were utilized together with ~1.6 · 10^6 t of cement. According to the information available to the constructors at the tender stage, the basalt from the excavation was adequate for this purpose. However, when the production of concrete for the first structures began, seven months after the beginning of the excavation, the problems became apparent. The crushing of the materials that had been stored for seven months under the tropical weather at the site resulted in rapid degradation of the basalt, and generation of a large quantity of fines. This forced to the constructors to modify the crushing plant and to look for a new source of raw materials for the concrete production, which in turn resulted in the delay in the construction and in the important overruns occurred.

Why did an apparently fresh and sound basalt, ordinarily used for construction, generate much more fines than expected? Why were the rocks coming directly from the quarries able to pass the mechanical test while the stored and processed rocks from the excavation had to be rejected? To answer these questions, an in-depth characterization of the representative rocks from the area was conducted.

2. Geological setting

The Isthmus of Panama is a geologically very complex area owing to its geotectonic position, at the convergence of the Caribbean, South America, Nazca, and Cocos plates. The interaction of these tectonic plates generated an island arc archipelago on the Mesozoic oceanic crust of the Caribbean plate (Silver et al., 1990; Mann and Kolarsky, 1995; Coates et al., 2004). Goldsmith et al. (2015) describe the lithology of the area as a "mosaic of bedrock lithologies including hydrothermally altered marine oceanic crust, intrusive igneous rocks of mafic to felsic composition, and an array of submarine and subaerial volcanic of tholeiitic, low-K calc-alkaline, and adakitic affinity." Unconformably upon these rocks, shallow-marine and volcanoclastic sediments were deposited. According to Stewart and Stewart (1980), in the Pacific area where the new Cocolí locks have been excavated, two lithologies appear (Fig. 1): the mainly sedimentary and siliciclastic La Boca Formation, early Miocene in age, and the Late Basalt Formation that comprises

* Corresponding author.
E-mail addresses: msuarez@usal.es (M. Suárez), mromero@ucm.es (E. García-Romero), mbaz@sacyr.com (A. Baz), rperez@sacyr.com (R. Pérez).

https://doi.org/10.1016/j.enggeo.2021.106036
Received 30 August 2020; Received in revised form 23 December 2020; Accepted 3 February 2021
Available online 6 February 2021

intrusive and extrusive basalts, from the middle and late Miocene (described in detail by Farris et al., 2017). The Late Basalt extends to the southwest of the canal on the Pacific side and is known as the MB in the locks area. In this area, major faults are present, such as the Pedro Miguel Fault and the Miraflores Fault, which cross the Panama Canal between the Pedro Miguel and Miraflores locks (Stewart and Stewart, 1980). These faults are part of a system of conjugate faults related to the accommodation of the internal deformation resulting from the ongoing collision of Central and South America (Rockwell et al., 2010).

3. Materials and methods

A wide group of representative samples from the excavation and from different quarries in the area were studied to understand their mineralogical composition, geochemistry, texture, and properties. The study comprised samples coming from the quarries used as the source of aggregates for the concrete and from the excavation of the new canal: i) 26 samples from Aguadulce Hill quarry labeled as AHQ, SPP1, and SPP2; 9 samples from Cocoli Hill quarry labeled as CHQ; ii) 4 samples from the excavation, labeled as LH and TRI; iii) a group of processed samples that comprises 2 samples from the temporal stockpile, labeled as PLE and 10 aggregates of ~40 mm size taken from the secondary crusher at the crushing plant labeled as CR. The location of the quarries, the crushing plant, and the temporary stockpile is in Fig. 2. The compositions and textures were studied by X-ray diffraction (XRD), optical mineralogy and petrography, scanning electron microscopy (SEM), and chemical analysis of major and trace elements. In addition, a selection of representative samples was also studied by microprobe. Finally, an experiment of accelerated aging was carried out to compare the behaviors of different samples.

The chemical analyses of major and trace elements were performed at Actlabs, the Activation Laboratory from Ontario (Canada). Actlabs is ISO 17025 accredited and/or certified to 09001:2008. The selected package of analysis was 4lithores-research that includes lithium metaborate/tetraborate fusion ICP. Fused sample is diluted and analyzed by Perlin Elmer Sciex ELAN 6000, 6100 or 9000 ICP/MS. Three blanks and five controls (three before the sample group and two afterwards) were analyzed per each group of samples. Duplicated were fused and analyzed every 15 samples, and the instruments were recalibrated every 40 samples (www.ctlabs.com).

The micro-morphological study was conducted using a field emission gum scanning electron microscope (SEM-FEG; JEOL JSM-6335F) at the Centro Nacional de Microscopía Electrónica (Madrid, Spain). The SEM-FEG observations were conducted with the microscope operating at 10 kV and a working distance of 15 mm. Prior to the SEM-FEG examination, freshly fractured surfaces of representative samples were air-dried and coated with Au in vacuum.

The mineralogical characterization was performed via XRD using a Siemens D-500 and a Bruker D8-Advance diffractometers equipped with a Cu-Kα radiation source, graphite monochromator, and 0.05° 2θ/3 s scan speed (in the Bruker equipment) and 0.05° 2θ/1 s scan speed (in the Siemens equipment). Samples used to determine the global mineralogy were random-powder specimens, and the procedure for clay minerals studies was the standard one, which comprises the following steps. Raw

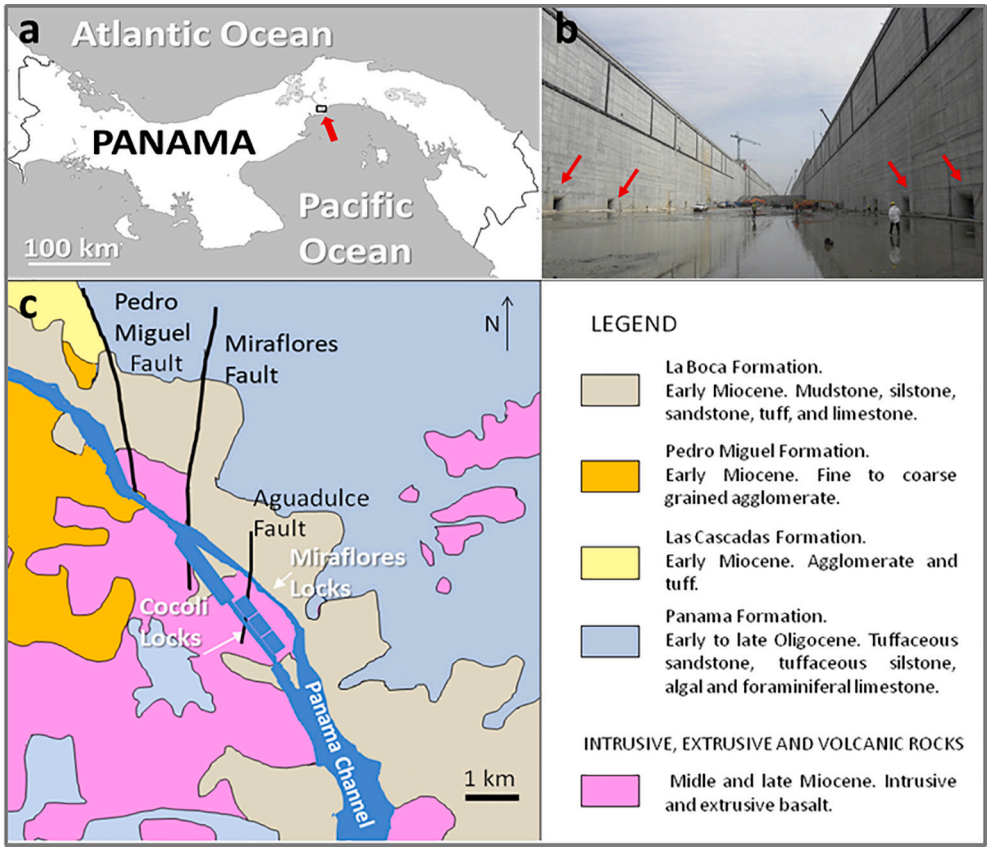

Fig. 1. a) Map of Panamá. Red arrow indicates the studied area. b) The new Cocoli Looks at the end of the construction, red arrows indicate where the water fills and empties the locks. c) Simplified geological map of the site, modified from Stewart and Stewart (1980). (For interpretation of the references to colour in this figure legend, the reader is referred to the web version of this article.)

samples: The powder XRD patterns were analyzed using X-pert High Score Plus software and EVA software and compared with the JCPDS database files. Obtaining the <2 μm fraction: 50 g of sample was put in suspension in 1.5 l of deionized water and agitated overnight. The <2 μm fraction was extracted following Stokes's law. With the suspension of the <2 μm fraction, the oriented aggregate on the surface of a glass slide was prepared. The oriented aggregates were scanned: in normal ambient conditions, after solvation with ethylene glycol to be able to identify swelling minerals of the smectite group, and after heating the sample at 550 °C for 2 h to be able to distinguish chlorites. Semi-quantification was done according to the reflective-powers method (Martín-Pozas, 1975).

The microprobe study on doubly-polished thin sections was performed at the ICTS-ELECMI (Centro Nacional de Microscopía Electrónica, Madrid) by using a JEOL Superprobe JXA-8900 M with WDS electron probe micro analyzer that allows to analyze from Be to U. The microprobe allows us to obtain very precise punctual analyses of the desired areas, even within the same mineral. It provides data to calculate the mineral structural formulae. Structural formulae of smectites was fitted for 22 negative charges.

Granulometric curves were obtained according to the (ASTM Standard C33, 2006).

Different representative samples were submitted to an accelerated aging experiment according to the standard (ASTM C88/C88M-18, 2018). Five aggregates of ~4 cm (sample CR-1) coming from the secondary crusher of the crushing plant built for on-site concrete fabrication, three samples from Aguadulce Hill quqarry, and three samples Cocoli Hill quarrie (Fig. 2 a, b). The samples from the quarries were cut with a diamond saw into cubes of 7 cm, 4 cm, and 2 cm per side, respectively, according to the sizes of the primary, secondary, and tertiary crushers at the crushing plant in Panama. 30 diary cycles were done with the next steps: 1) samples are immersed for 4 h in a dissolution $Na_2SO_4 \cdot 10H_2O$ at 14%, after that they are dried at 60 °C for 16 h, and finally, the samples stay other 4 h at ambience temperature before than restart the cycle. At the end of each cycle all samples are weighted and subjected to a visual inspection photographing and noting the observed changes.

4. The miraflores basalt

The Miraflores Basalt (MB) is the formation where most of the excavation for the third set of locks on the Pacific side was carried out (cf. the geological setting in GSA Data Repository). The quarries used as

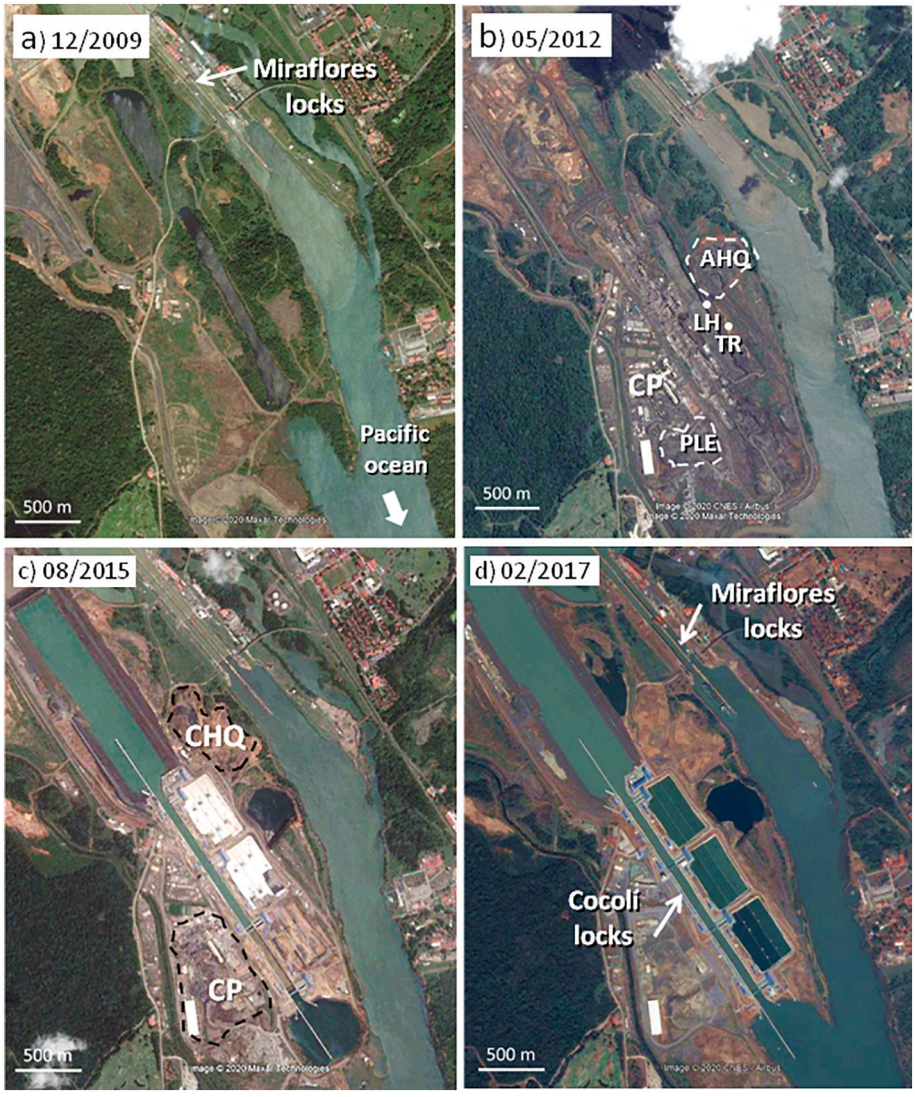

Fig. 2. Satellite images (© Google Earth) of the site that show the evolution of the third set of locks of the Panama Canal construction. Location of sampling, quarries, and crushing plant area. a) The site before than start the works for the construction of the new locks. b and c) two different views during the construction. AHQ: Aguadulce Hill quarry, LH and TRI: places of sampling in the excavation. CP: crushing plant area. PLE: stockpile area for the crushing plant. CHQ: Cocoli Hill quarry. d) Cocoli locks view.

rock-source for aggregates and sand fraction for concrete are also in the MB (Figs. 1, 2, and 3). The rocks in the MB range from microgabbro to diabase, and are mostly formed by plagioclases, between oligoclase and bytownite, pyroxenes (ordinarily augite), and minor amounts of olivine and titanomagnetite, as primary minerals (Fig. 4). The phenocrysts are mainly euhedral and sometimes aligned plagioclases, while the pyroxenes appear primarily as sub- to anhedral crystals among and around the plagioclases (Fig. 4b, d, g). This is, according to Farris et al. (2017), a distinctive characteristic that allows to differentiate the Late Basalt from the Pedro Miguel basaltic lava flows that also outcrop in the area. Variable proportions of devitrified volcanic glass also appear in all studied rocks (Fig. 4 and 5a, b, c) and, at times, the glass contains idiomorphic apatite crystals (Fig. 5a). Based on the chemical composition (Table 1) and using the TAS diagram (Le Maitre et al., 2002), the rocks are classified as ranging between basaltic andesite and basalt (Fig. 6). According to the iron content, the basalts are classified as tholeiitic.

Two types of alteration of the basalt can be identified in the area. The MB is affected by the circulation of hydrothermal fluids and millimetric to centimetric veins filled by smectites are frequent. On the other hand, reed tropical soils, rich in kaolinite and Fe-oxides as product of the basalt weathering, are developed. Both the olivine and the glass are completely altered to iddingsite (Fig. 4c, d) and palagonite (Fig. 5a, e), respectively, and these two alteration products are mainly composed of smectites together with minor amounts of Fe-oxides that appear as opaque minerals in Fig. 4a, c, e). Iddingsite begins to form since the early stages of basalt formation (Eggleton, 1984; Banfield et al., 1990), while the palagonite results from glass alteration (Stroncik and Schmincke, 2002) as a result of the circulation of hydrothermal fluids associated to the tectonic activity in the area. In addition, both plagioclases and pyroxenes appear altered to smectites within the crystals and at their edges (Figs. 4e and 5b, c, d, e). Consequently, overall, the smectites are major mineral components in the rock (~17% mean content) and have indeed been identified in all XRD patterns (Fig. 7). Smectites (mainly saponite or Fe-bearing saponite) have been recognized as the main product of basalt alteration at low temperature since the first studies by Loughnan (1969), Böhlke et al. (1981), and Eggleton et al. (1987). Nevertheless, the composition of the smectites obtained from microprobe analysis in the MB suggests that they are rich in high-charge Fe-rich beidellites, consistently with the d060 spacing in the powder XRD pattern found at 1.49 Å. The structural formula fitted for the mean values of the chemical composition of 372 analyses is: $(Si_{3.47}\ Al_{0.53})\ O_{20}\ (Ti_{0.02}\ Al_{0.15}\ Fe^{3+}{}_{1.08}\ Mg_{1.06})\ (OH)_4\ Ca_{0.18}\ Na_{0.17}\ K_{0.12}$. The presence of Fe-rich dioctahedral smectites rather than saponite (a trioctahedral Mg-rich smectite) as the alteration product of a basic rock is not common. Nonetheless, Fe-rich dioctahedral smectites have been found in other altered basalts (Giorgetti et al., 2009; Rasmussen et al., 2010; Fontaine et al., 2020). Their presence is considered an evidence of an "open microsystem" with moderate leaching, where the interaction of the Mg-phases with neighboring plagioclases results in the formation of Al-bearing smectite (Vingiani et al., 2010). Gaudin et al. (2018) related the formation of dioctahedral instead of trioctahedral smectite to the presence of CO_2. This may have occurred also in the MB, a hypothesis that is corroborated by the late calcite precipitation in micrometer and millimeter fractures (Fig. 4g, h).

5. Smectites texture and microtexture

Because of the tectonic activity and the fault zones, the rocks are micro- and nano-fractured (Fig. 8). Under petrographic microscope, a network of micro-cracks can be seen, which crosses the rock and is connected by a dense network of nano-cracks breaking the pyroxene and plagioclase crystals. Occasionally, quartz or chalcedony and calcite fill up the millimetric fractures. However, the clay minerals visible under petrographic microscope, owing to the Fe-oxides associated with them and their anisotropy, are widespread, and fill both the micro- and the nano-cracks (Figs. 4c, d, e, f and 8a, b, d). The XRD patterns indicate that smectites are the sole clay minerals present in all the studied samples from the MB (Fig. 7); therefore, the clay minerals filling the micro- and

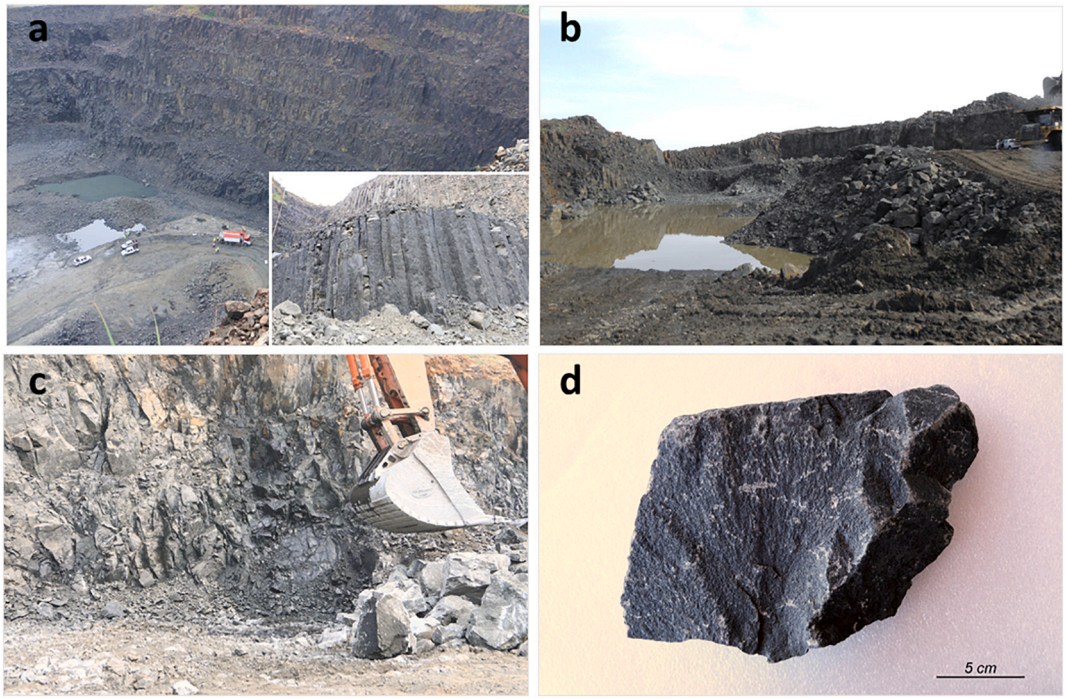

Fig. 3. a) Aguadulce Hill quarry general view and detail of the columnar disjunction. b) Cocoli Hill quarry. c and d) Basalt from the Cocoli Hill quarry.

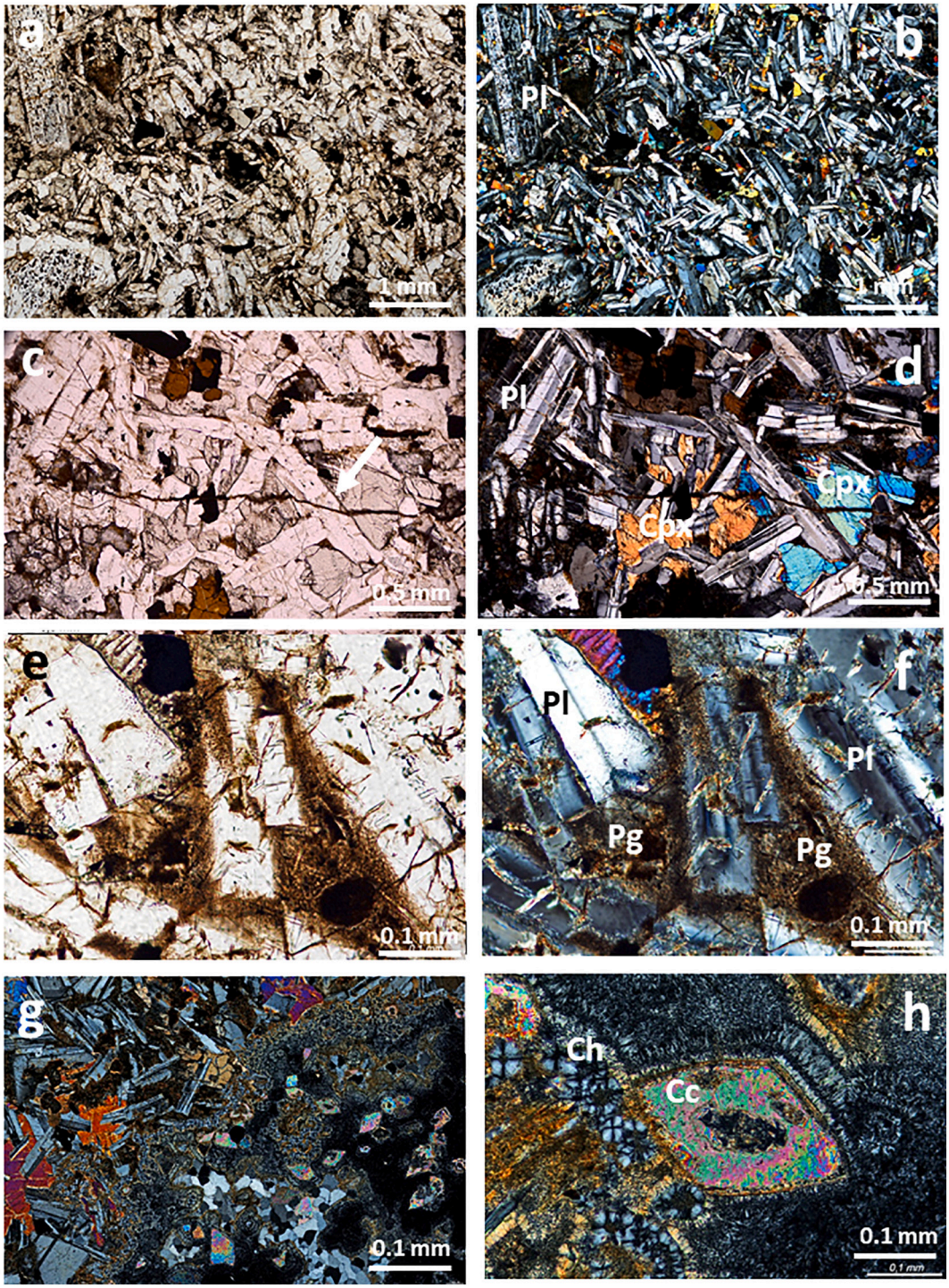

Fig. 4. Optical images of Miraflores Basalts. a–b) General view of the studied rock. It is composed by sub-idiomorphic plagioclase, and minor clinopyroxene crystals included in an anisotropic matrix. c–d) The same rock observed with higher magnification. It is possible to observe the fractures. Big cracks filled by smectites cross throughout the rock and minor cracks cross the crystals. e–f) Detail of the rock where it is clear the relation among smectites and plagioclase crystals. Note as the smectites cover the edges of the crystals and corrode their surfaces and they penetrate in the fractures that cross the rock. g) Detail of the contact between the volcanic rock (at the upper left corner) and a vein filled by chalcedony and calcite which have growth in several stages. h) Detail of the vein that shows chalcedony and calcite (sparite crystals) formed in successive stages of growth. Cpx: Clinopyroxene, Pl: plagioclase. Pg: palagonite. Ch: Chalcedony. Cc: Calcite (sparite crystals).

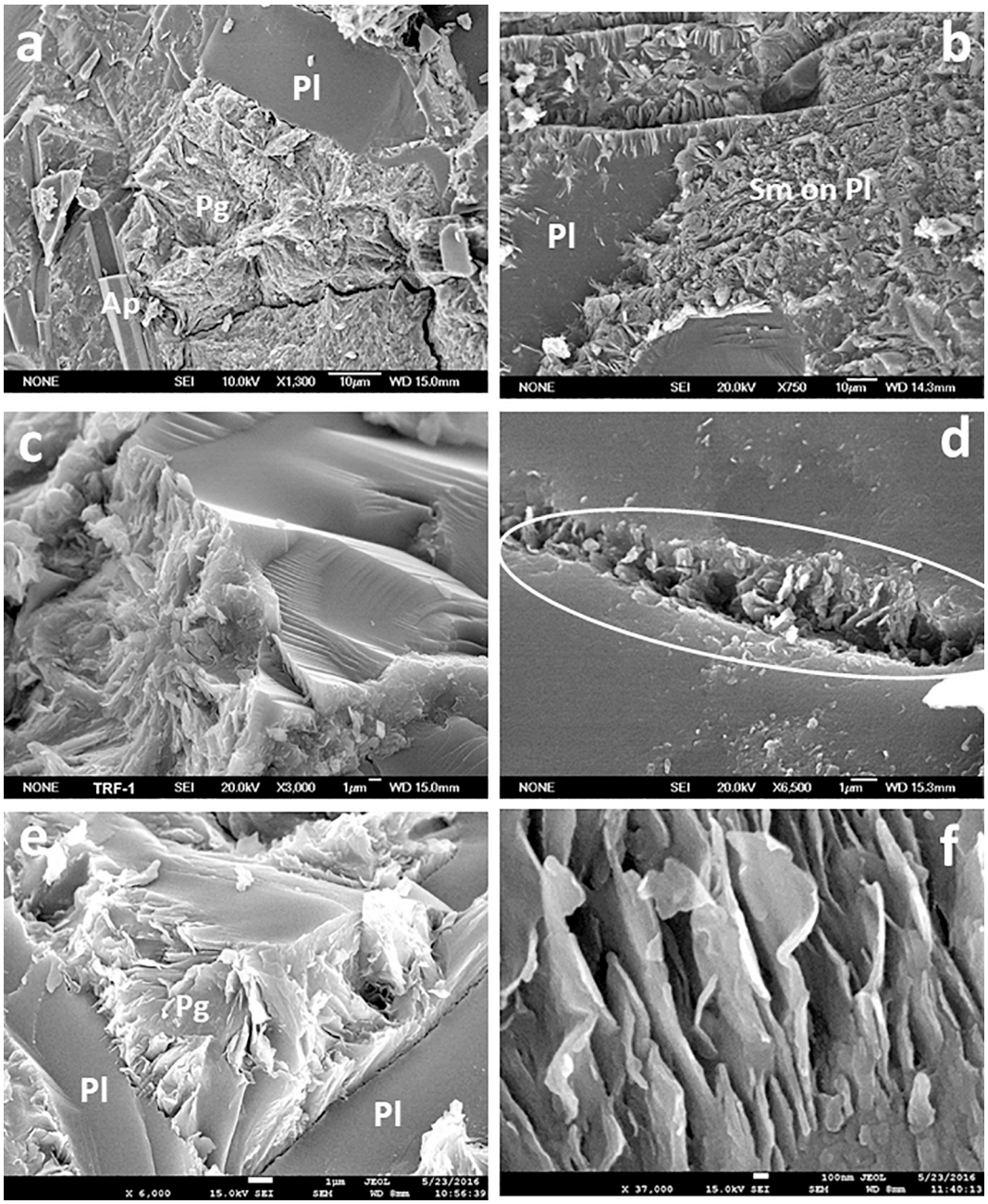

Fig. 5. Scanning Electron Microscopy images. a) General view. The plagioclase and apatite idiomorphic crystals are included in the palagonitic matrix. b) Plagioclase crystal covered by smectite which growths on its surface. c) Edge of smectite crystal where the palagonite is growing. d) Smectites on the contact surface between two plagioclase crystals. e) Palagonite growing among plagioclase crystals. f) Epitaxial growth of smectite on the clinopyroxenes cleavage. Ap: Apatite. Pl: Plagioclase. Pg: Palagonite. Sm: Smectite.

Table 1
Chemical composition of the studied samples, in % weigh of major elements. AHQ, SPP1, and SPP2: Aguadulce Hill quarry, CCH: Cocoli Hill quarry, LH nad TRI: excavation of the canal, CR: aggregates from the crushing plant, PLE: stockpiled material.

Location	Sample	SiO_2	Al_2O_3	Fe_2O_3	FeO	MnO	MgO	CaO	Na_2O	K_2O	TiO_2	P_2O_5	LOI
AHQ	566-1A	52.35	15.52	4.02	5.70	0.18	4.49	8.17	3.64	0.70	1.78	0.45	2.15
AHQ	566-2	52.99	15.93	3.26	6.70	0.18	4.53	8.17	3.72	0.80	1.66	0.47	1.23
AHQ	566-3	52.24	16.20	3.45	6.70	0.18	4.42	8.46	3.69	0.78	1.65	0.47	1.28
AHQ	566-4	51.66	16.31	3.25	6.60	0.19	4.45	8.60	3.59	0.77	1.72	0.43	1.51
AHQ	566-5A	52.17	15.85	3.35	6.80	0.18	4.45	8.50	3.63	0.78	1.69	0.44	1.28
AHQ	566-6	52.74	16.21	3.15	6.90	0.18	4.46	8.56	3.66	0.81	1.64	0.45	1.22
AHQ	AHQ1	52.95	16.08	3.47	6.40	0.17	4.58	8.66	3.67	0.67	1.59	0.41	1.40
AHQ	AHQ-1B	50.96	16.27	3.78	6.70	0.18	4.22	8.63	3.47	0.67	1.60	0.39	1.23
AHQ	AHQ-2	51.85	16.67	4.01	5.50	0.16	4.55	8.57	3.48	0.65	1.41	0.37	2.17
AHQ	AHQ-2B	52.62	15.66	3.56	6.40	0.18	4.18	8.58	3.49	0.83	1.62	0.43	1.50
AHQ	AHQ-3	52.04	15.85	3.63	6.50	0.17	4.37	8.24	3.59	0.70	1.42	0.42	1.50
AHQ	AHQ-3B	51.09	15.77	4.18	6.00	0.17	4.28	8.61	3.45	0.68	1.59	0.41	1.77
AHQ	SPP1	50.29	16.78	4.71	4.80	0.16	4.80	9.77	3.42	0.46	1.38	0.34	2.56
AHQ	SPP2	51.14	16.77	4.99	4.90	0.12	4.43	9.11	3.37	0.56	1.53	0.38	2.79
CCH	567-1	49.56	17.26	4.38	5.30	0.16	4.54	9.49	3.14	0.55	1.53	0.35	3.18
CCH	567-2	50.01	17.22	4.68	4.90	0.17	4.81	9.55	3.20	0.23	1.48	0.37	3.47
CCH	567-3A	51.31	15.86	4.07	5.70	0.17	4.44	8.75	3.51	0.69	1.61	0.42	2.43
CCH	567-4	49.47	17.20	5.34	4.20	0.15	4.84	9.22	3.13	0.50	1.47	0.38	3.99
CCH	567-5	49.31	17.16	4.26	5.00	0.16	5.15	9.90	3.16	0.51	1.41	0.35	3.50
CCH	567-6A	50.31	16.23	2.37	7.20	0.17	5.08	9.12	3.39	0.56	1.53	0.37	2.97
CCH	CCH-1	52.98	16.01	2.95	7.00	0.18	4.56	8.44	3.76	0.73	1.67	0.45	1.25
CCH	CCH-2	51.92	16.40	3.63	6.50	0.17	4.45	8.73	3.56	0.67	1.59	0.42	1.24
CCH	CCH-3	53.64	15.81	2.92	7.00	0.18	4.42	8.15	3.83	0.81	1.62	0.44	1.20
LH	LH-1	52.95	16.01	3.08	6.80	0.17	4.44	8.35	3.58	0.77	1.52	0.42	1.00
LH	LH-2	53.24	16.16	3.22	6.50	0.18	4.47	8.47	3.64	0.73	1.62	0.44	0.94
TRI	TRF-1	51.81	15.88	4.26	5.70	0.18	4.62	8.98	3.34	0.61	1.52	0.40	2.22
TRI	TRF-1	51.03	15.96	5.06	5.10	0.17	4.71	8.93	3.36	0.56	1.52	0.35	2.95
SPP1	573-1A	52.43	16.50	3.26	6.20	0.17	4.52	8.62	3.67	0.69	1.56	0.40	1.31
SPP1	573-2A	51.82	15.87	4.52	5.80	0.18	4.70	8.28	3.42	0.75	1.66	0.44	2.48
SPP1	573-3A	51.93	15.86	3.40	6.50	0.16	4.49	8.61	3.48	0.67	1.55	0.41	2.19
SPP1	573-4A	52.51	15.24	3.16	6.90	0.16	4.47	8.30	3.53	0.73	1.66	0.45	2.16
SPP1	573-5A	53.06	14.27	3.46	6.90	0.18	4.40	8.71	3.73	0.72	1.75	0.46	1.26
SPP1	573-6A	50.72	17.11	3.69	5.30	0.16	4.94	9.89	3.28	0.50	1.38	0.36	2.47
SPP2	574-1B	49.72	17.55	4.78	4.60	0.15	4.82	9.23	3.28	0.56	1.50	0.37	3.67
SPP2	574-2A	49.94	16.62	4.53	4.60	0.15	4.58	9.32	3.23	0.55	1.46	0.35	3.19
SPP2	574-3A	49.76	16.10	4.69	5.20	0.15	5.34	9.35	3.08	0.47	1.48	0.39	3.73
SPP2	574-4	51.14	16.60	3.86	5.70	0.17	4.33	9.27	3.31	0.57	1.48	0.35	2.82
SPP2	574-5B	51.40	16.78	3.79	4.60	0.15	4.39	9.93	3.21	0.49	1.27	0.29	2.95
SPP2	574-6A	48.55	17.05	5.57	5.40	0.14	5.07	9.52	3.07	0.24	1.47	0.30	3.79
CR	CR-1	49.06	16.73	5.10	4.30	0.165	4.77	9.24	3.23	0.48	1.42	0.35	3.73
CR	CR-2	48.81	17.26	5.15	3.80	0.146	5.00	9.72	3.19	0.44	1.35	0.31	3.84
PLE	PLE-1	50.05	17.53	5.33	3.60	0.147	5.08	9.88	3.25	0.41	1.24	0.33	3.49
PLE	PLE-2	49.31	17.64	4.32	4.30	0.131	5.02	9.08	3.45	0.42	1.23	0.30	3.27

nano-cracks are certainly smectites. Under SEM, smectites are observed not only in iddingsite and palagonite, and filling micro- and nano-cracks (Fig. 5,d and 8a,b,d), but also replacing plagioclases and pyroxene crystals and growing on their surfaces (Figs. 5b, c, d, e and 8c, d), sometimes with a topotactic relationship (Fig. 7f), as well as within these crystals as a product of their alteration (Figs. 5e, and 8d).

The presence of smectites, therefore, is not only limited to the iddingsite and palagonite: they are also found around plagioclase and pyroxene crystals and filling the dense network of micro- and nano-cracks in such a manner that not only there is a significant amount of smectites, but these smectites are also intensely connected (Fig. 8d). This connection is the key to explaining the unexpected behavior of the stockpiled rocks, and that of the freshly excavated basaltic rocks when they are processed in the crushing plant.

The characteristics of the MB change from the mass-rock, where the network of cracks is balanced and sealed by smectites, to the obtention of aggregates and sands used for concrete production, where the cracks are weakened and open allowing the smectites swell in contact with water. Owing to the weakening and opening of the micro- and nano-cracks resulting from blasting, transport, storage, and crushing, the mechanical properties of the rock change. The strength of the altered igneous rock is therefore much lower than that of the unaltered igneous crystals because the contact surfaces among these crystals are covered by smectites (Figs. 5d and 8c, d).

During crushing, the rocks break along the weakened network of micro- and nano-cracks filled by smectites. As a result, the smectites filling these cracks and covering the crystal surfaces come into contact with water and are released by dispersion and suspension (Fig. 9). This, in turn, allows the separation and release of crystals and portions of crystals of primary minerals, resulting in a much higher loss of fines than expected. The granulometric curve of the sand obtained after basalt crushing at the beginning of concrete production (discontinuous red line in Fig. 10) crosses the lower limit of the granulometric spindle at the point corresponding to >55% of particles with size <0.5 mm. This implies that a very large amount of superfine sands had to be disposed as waste. The superfine sands recovered by cyclone extraction are enriched in plagioclase and pyroxenes (Fig. 11) occurring as small particles (size < 600 μm as schematized in Fig. 9c) because a certain proportion of the finest particles, the smectites, had been lost in the suspension.

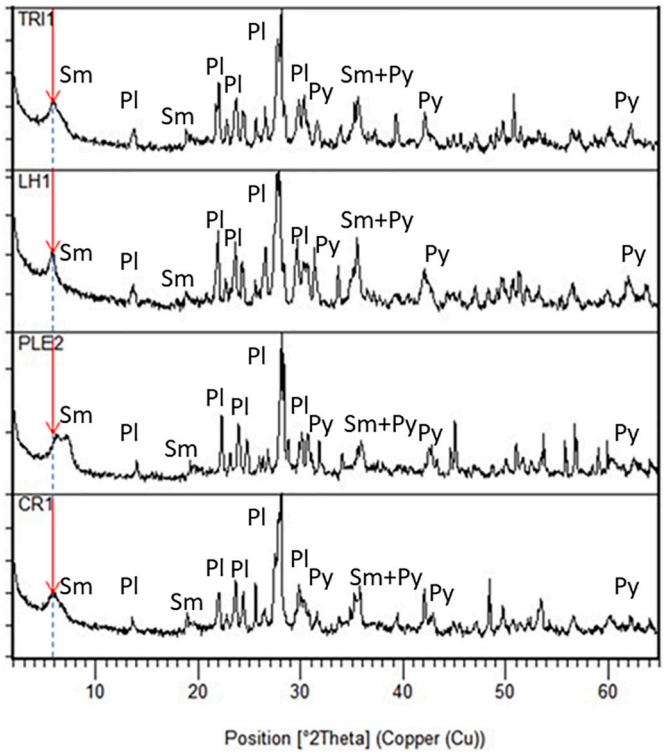

Fig. 7. Powder X-Ray diffraction patterns of some representative samples. Red arrow indicates the 001 reflection of the smectites. (For interpretation of the references to colour in this figure legend, the reader is referred to the web version of this article.)

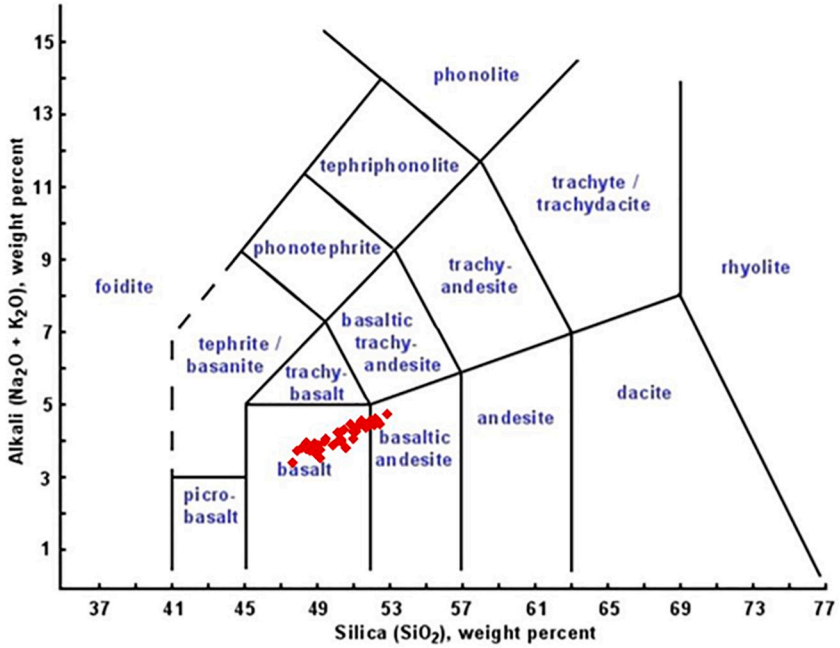

Fig. 6. Projection of the chemical composition of the samples in the TAS diagram.

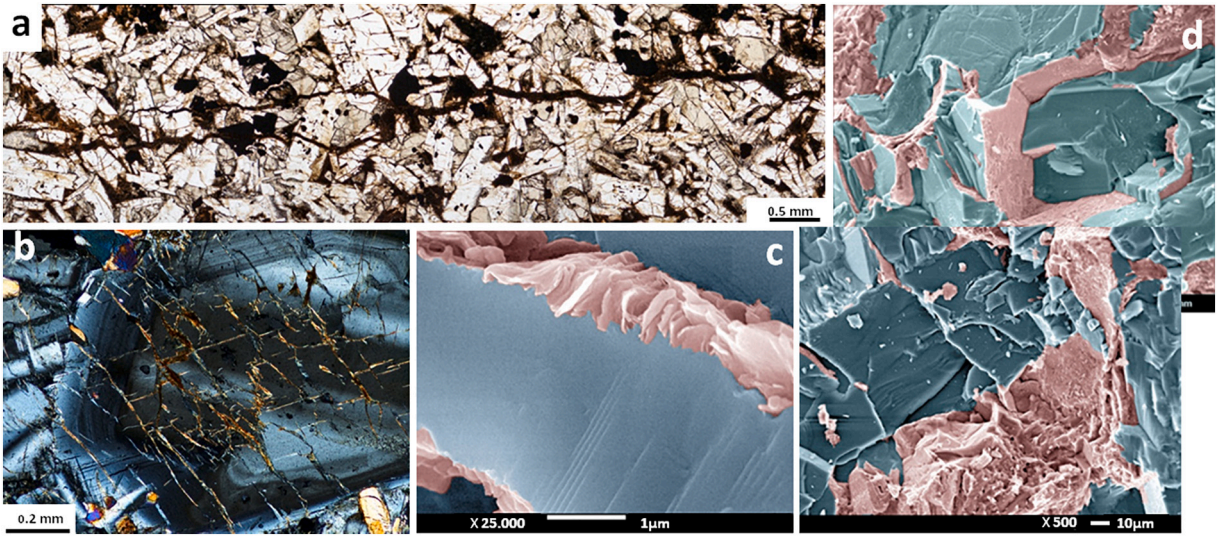

Fig. 8. Images of the Miraflores Basalt. a) and b) Photomicrographs illustrating the micro- and nano-cracks of the rock. In a), note the horizontal micro-crack through the rock as well as other micro- and nano-cracks crossing the crystals. In b), a plagioclase crystal is shown. Note the dense network of nano-cracks filled by smectites crossing the crystal along two main directions. c) and d) False-colour scanning electron microscopy images. Gray: plagioclase crystals, pink: smectites. c) Plagioclase crystal, the edges of which are altered and covered by smectite crystals. d) Intensely fractured plagioclase crystal with surfaces covered by smectites; all nano-cracks are filled by smectites. Note that these smectite crystals are interconnected. (For interpretation of the references to colour in this figure legend, the reader is referred to the web version of this article.)

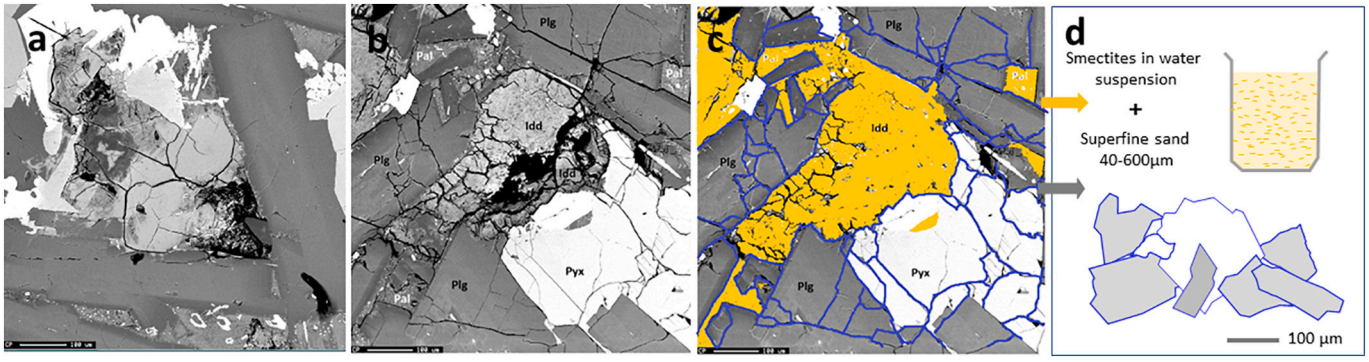

Fig. 9. a) Microprobe image of a sample from Aguadulce Hill quarry b) Microprobe image of a sample from the same quarry after crushing; the opening of the micro- and nano-cracks is visible; Plg: plagioclase, Pyx: pyroxene, Idd: iddingsite, and Pal: palagonite. c) The same image with smectites coloured in orange and open surfaces in blue. d) Schematic image showing the formation of superfine sand enriched in primary minerals that breaks through the fractures (blue lines in c), and the leaching of smectites in water suspension. (For interpretation of the references to colour in this figure legend, the reader is referred to the web version of this article.)

Knowing the presence of smectites and their texture help us to understand why the MB produced much more fine particles than expected. However, this does not explain why the same behavior was not observed prior to the beginning of construction. In the case of the rocks stockpiled from the beginning of the excavation until the beginning of concrete production (up to seven months), blocks of blasted rock remained exposed to the Panamanian climate for months, subjected to daily changes of temperature and humidity. Water was able to penetrate throughout the network of cracks weakened by blasting, thereby triggering a cyclic swelling and shrinking of the smectites that further weakened the rock and reduced its cohesion. In other words, the rocks from the excavation underwent weathering and underwent rapid degradation which was facilitated by the access of water into the rock interior through the network of open cracks (Fig. 9).

The Panamanian climate is characterized by dry-wet cycles on an almost daily basis. Under such conditions, the smectites contained in the stockpiled rock fragments, which have a much larger exposed surface than the rock in the quarry, undergo cyclic swelling and shrinking that weaken the rocks. According to Higgs (1976), the swelling pressures due to the water absorption by smectites in an altered basalt could exceed 14 MPa. This was observed in the studied rocks; in fact, when rocks from the quarries and from the stockpile were compared, a clear difference was observed. The mean compressive strength of the rocks from the quarries and the excavation was 82.33 MPa, while that of the rocks from the stockpile was 50.08 MPa. The process of rapid degradation of basic igneous rocks when exposed and used as a construction material is not frequent and has never been investigated in depth, even though it has been recorded at a few locations, mainly in South Africa (Orr 1979; Bell and Jermy, 2000; Leyland et al., 2015).

6. Accelerated aging

The alteration of the stockpiled rocks in a very short time can explain why they could not be used to produce aggregates and the constructors had to look for a new source of materials using the basalt directly from the quarries and avoid stockpiling. However, this cannot explain why the same rapid alteration does not occur at the quarries or in natural outcrops. In order to shed light onto such different behaviors of the same rocks, an accelerated aging experiment was carried out by comparing the rock from the quarry without blasting with the aggregates obtained

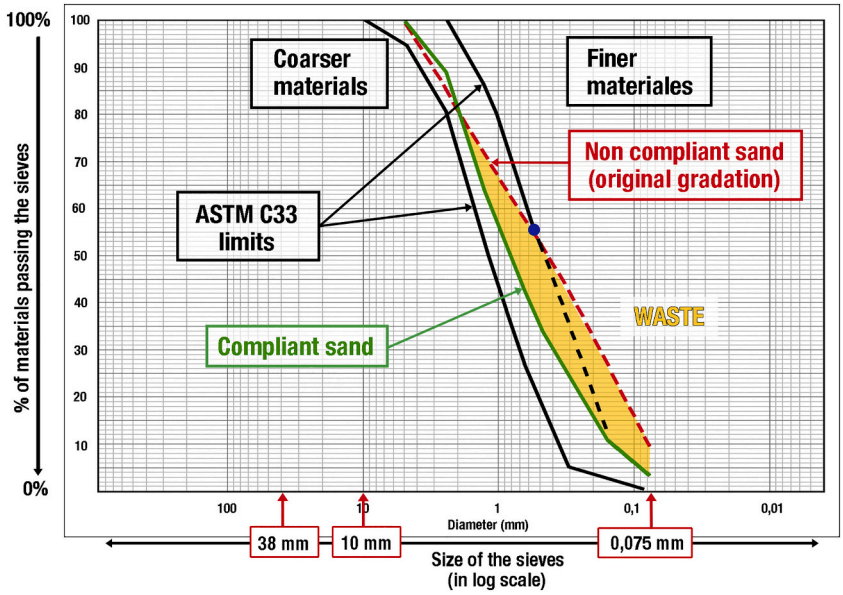

Fig. 10. Sand gradation during the first crushing plant operation in January 2011: in orange, the non-compliance material (superfine sand) is indicated. (For interpretation of the references to colour in this figure legend, the reader is referred to the web version of this article.)

from the same quarry, which were obtained through a sequence of industrial process including blasting, transport, and crushing. The behavior of the basalt taken directly from the quarry was completely different from that of the basalt aggregates during the aging experiment (Fig. 12). The rocks from the quarry exhibited only minor changes after 30 days, with a change in colour due to the oxidation of Fe^{2+} and the opening of one crack. Conversely, the aggregates disintegrated within 3 to 5 days.

Both rocks did not undergo stockpiling. Therefore, the different behaviors must arise from the different processes underwent by the aggregates. In addition to blasting and transport from the quarry, the rock fragments of the aggregates are also subjected to mechanical stresses during different production stages at the crushing plant. If the basalt does not have a dense network of micro- and nano-cracks filled by smectites as in the MB, the sequence of these processes does not cause issues. This is indeed the typical response of most basalts used in construction around the world, for which weathering only occurs in geological time from the outside to the inside of the rock (Fig. 13). However, in our case, the network of fractures weakened and opened during each step of the production process, leading to a significant loss of mechanical properties and facilitating the decomposition of the rock.

7. Final remarks

The rapid degradation during the industrial process of an apparently *sound basalt* was due to: 1) the presence of smectites in a dense network of micro- and nano-cracks breaking through the rock, and 2) to its weakening due to the processes of blasting, transport, storage, and crushing. These processes opened the network of natural fractures filled by smectites and facilitated the access of the water into the rock and the swelling of these clay minerals. As aforementioned, the explanation was simple, yet not easily detectable. The key of the problem was not the presence of smectites – which can occur in basalts used for aggregates production – but in their texture. If smectites in altered basalt are confined to the iddingsite, for instance, they remain encapsulated into the igneous rock and cannot be accessed by water. In the MB, highly

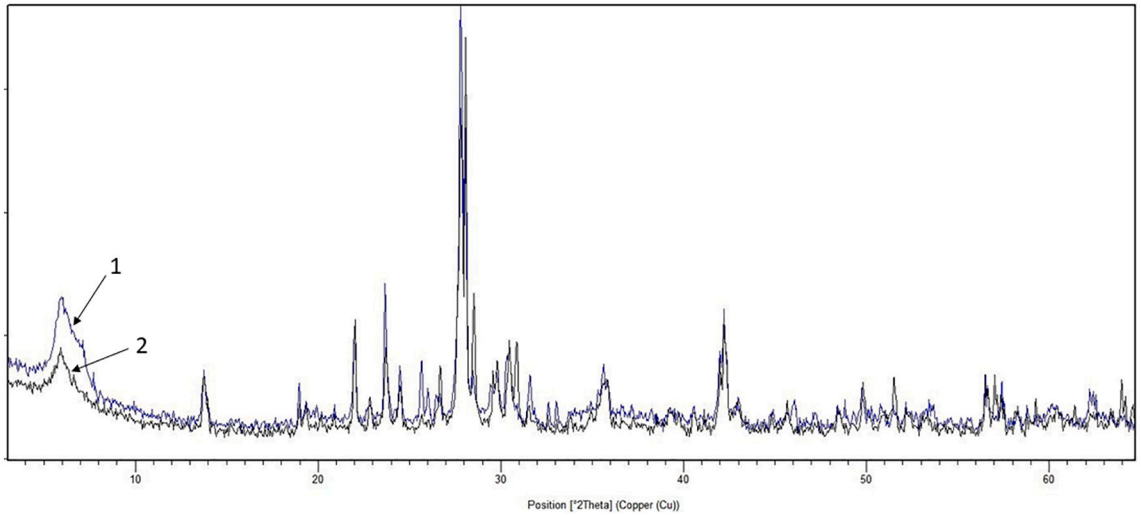

Fig. 11. Powder X-Ray diffraction patterns of 1) a representative sample from the Aguadulce Hill quarry. 2) superfine sand. Numbers indicate the 001 reflection of the smectites, note the lower intensity of this reflection in the superfine sand sample.

Fig. 12. Accelerated aging pictures. a) Samples from the Aguadulce Hill quarry (7 cm, 4 cm, and 2 cm side cubes) before the experiment of aging.; b) the same samples after 20 cycles. A change in colour from grey to brown and the opening of a major crack is observed; c) and d) aggregates from the crushing plant after 3 cycles: they are disaggregated and can be broken with fingers. (For interpretation of the references to colour in this figure legend, the reader is referred to the web version of this article.)

interconnected the smectites can break the rock down, even though their presence is not detectable even by optical microscopy. These nano-minerals are inert in the bulk rock under stable hydration conditions, but they are *awake* under the sum of the industrial processes in presence of water.

The results show that not only the presence but also the texture of the smectites – nano-minerals with particular swelling properties in contact with water – were responsible for the rapid degradation of the apparently fresh basaltic rock at the stockpile and for the high loss of fines during the industrial process. Although smectites are common products of deuterian and hydrothermal alteration of basalt and other basic igneous rocks, these rocks are frequently used as construction materials owing to their mechanical properties and durability. However, only a small proportion of smectites can trigger rock deterioration when they are highly interconnected. This process of rapid degradation of basic igneous rocks when they are exposed and used as construction

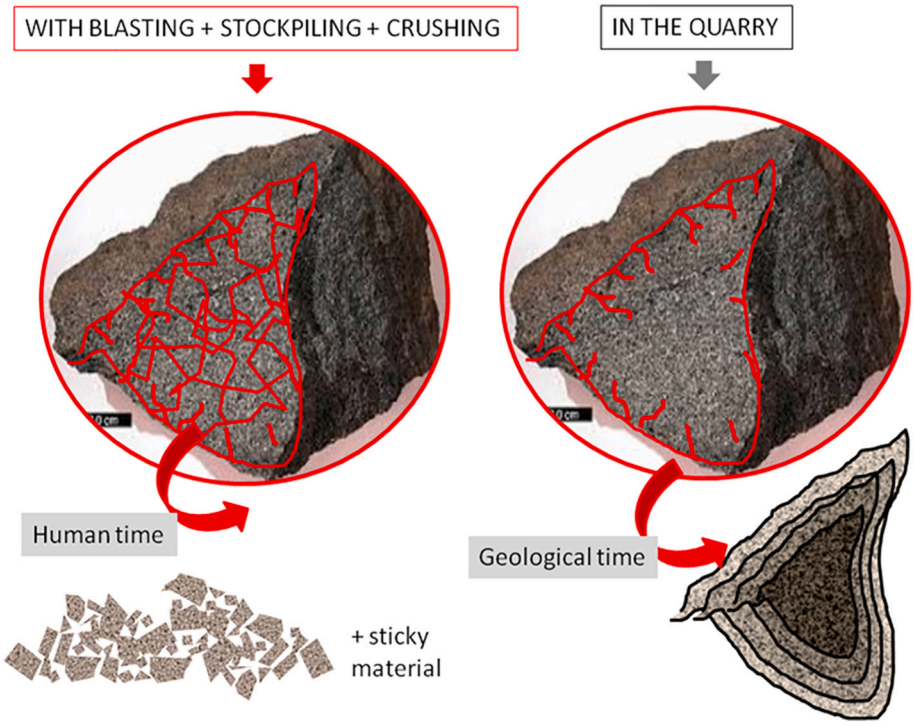

Fig. 13. Scheme of the different alteration paths. Left: progression of the alteration trough the weakened network of micro and nanocracks during the industrial process. Right: progression of the alteration in the natural environment.

material is not frequent, but it is significant enough to require the development of a new standard for the use of these materials in construction.

CRediT authorship contribution statement

Mercedes Suárez: Conceptualization, Investigation, Writing - original draft, Writing - review & editing, Supervision. **Emilia García-Romero**: Conceptualization, Investigation, Writing - original draft, Writing - review & editing. **Ascensión Baz**: Conceptualization, Resources, Writing - review & editing. Rafael Pérez: Conceptualization, Resources, Writing - original draft.

Declaration of Competing Interest

Two authors are working for Sacyr, one of the companies that formed the consortium that built the third set of locks of the Panama Canal.

Sacyr supplied the access the area and allow us the sampling.

A part of the data exposed in the manuscript was used in the paid expert testimony given in 2019 January.

Acknowledgements

The authors gratefully acknowledge the staff of the Fisheries Research Institute of Karatsu for their fish care and assistance during fish sampling. This work was supported by Grants-in-Aid for Scientific Research [KAKENHI: JP17K15322] for H.O.

References

ASTM C88/C88M-18, 2018. Standard Test Method for Soundness of Aggregates by Use of Sodium Sulfate or Magnesium Sulfate. ASTM International, West Conshohocken, PA.

ASTM Standard C33, 2006. Specification for Concrete Aggregates. ASTM International, West Conshohocken, PA.

Banfield, J.F., Veblen, D.R., Jones, B.F., 1990. Transmission electron microscopy of subsolidus oxidation and weathering of olivine. Contrib. Mineral. Petrol. 106, 110–123.

Bell, F.G., Jermy, C.A., 2000. The geotechnical character of some South African dolerites, especially their strength and durability. Q. J. Eng. Geol. Hydrogeol. 33, 59–76.

Böhlke, J.K., Honnorez, J., Honnorez-Guerstein, B., Muehlenbachs, K., Petersen, N., 1981. Heterogeneous alteration of the upper ocean crust: correlation of rock chemistry, magnetic properties, and O isotope ratios with alteration patterns in basalts from site 396B, DSDP. J. Geophys. Res. 86 (B9), 7935–7950.

Coates, A.G., Collins, L.S., Aubry, M., Berggren, W.A., 2004. The geology of the Darien, Panamá, and the Late Miocene–Pliocene collision of the Panamá arc with northwestern South America. Geol. Soc. Am. Bull. 116, 1327–1344.

Eggleton, R.A., 1984. Formation of iddingsite rims on olivine: a transmission electron microscope study. Clay Clay Miner. 32, 1–11.

Eggleton, R., Foudoulis, A., Varkevisser, C., D., 1987. Weathering of basalt: changes in rock chemistry and mineralogy. Clay Clay Miner. 35, 161–169.

Farris, D.W., Cardona, A., Montes, C., Foster, D., Jaramillo, C., 2017. Magmatic evolution of Panama Canal volcanic rocks: a record of arc processes and tectonic change. PLoS One 12, e0176010.

Fontaine, F., Christidis, G.E., Yans, J., Hollanders, S., Hoffman, A., Fagel, N., 2020. Characterization and origin of two Fe-rich bentonites from Westerwald (Germany). Appl. Clay Sci. 187 (art. no. 105444).

Gaudin, A., Dehouck, E., Grauby, O., Mangold, N., 2018. Formation of clay minerals on Mars: Insights from long-term experimental weathering of olivine. Icarus 311, 210–223.

Giorgetti, G., Monecke, T., Kleeberg, R., Hannington, M.D., 2009. Conical Seamount, Papua New Guinea: Formation of smectite and metastable precursor phases. Clay Clay Miner. 57, 725–741.

Goldsmith, S.T., Berry Lyons, W., Harmon, R.S., Harmon, B.A., Carey, A.E., McElwee, G. T., 2015. Organic carbon concentrations and transport in small mountain rivers, Panama. Appl. Geochem. 63, 540–549.

Higgs, N.B., 1976. Slaking basalts. Bull. Int. Assoc. Eng. Geol. 28, 287–302.

Le Maitre, A., Streckeisen, B., Zanettin, M., Le Bas, B., Bonin, B., Bateman, P. (Eds.), 2002. Igneous Rocks: A Classification and Glossary of Terms: Recommendations of the International Union of Geological Sciences Subcommission on the Systematics of Igneous Rocks (pp. X–Xii). Cambridge University Press, Cambridge, 236 pp.

Leyland, R.C., Verryn, S., Momayez, M., 2015. Smectite clay identification and quantification as an indicator of basic ingneos rock durability. Bull. Eng. Geol. Environ. 74, 981–989.

Loughnan, F.C., 1969. Chemical Weathering of the Silicate Minerals. Elsevier, New York, 154 pp.

Mann, P., Kolarsky, R.A., 1995. East Panamá deformed belt: structure, age, and neotectonic development. In: Mann, P. (Ed.), Geologic and Tectonic Development of the Caribbean Plate Boundary in South Central America, 295. Spec. Pap. Geol. Soc. Am., pp. 111–130

Martín-Pozas, J.M., 1975. Analisis cuantitativo de fases cristalinas por DRX. In: Saja, J. (Ed.), Método de Debye-Scherrer. ICE Universidad de Valladolid, Valladolid, Spain, pp. 77–89.

Orr, C.M., 1979. Rapid weathering dolerites. Civil Eng. South Africa 21, 173–225.

Rasmussen, C., Dahlgren, R.A., Southard, R.J., 2010. Basalt weathering and pedogenesis across an environmental gradient in the southern Cascade Range, California, USA. Geoderma 154, 473–485.

Rockwell, T., Gath, E., González, T., Madden, C., Verdugo, D., Lippincott, C., Dawson, T., Owen, L.V., Fuchs, M., Cadena, C., Williams, P., Weldon, E., Franceschi, P., 2010. Neotectonics and paleoseismology of the Limón and Pedro Miguel faults in Panamá: earthquake hazard to the Panamá Canal. Bull. Seismol. Soc. Am. 100, 6. https://doi.org/10.1785/0120090342.

Silver, E.A., Reed, D.L., Tagudin, J.E., Heil, D.J., 1990. Implications of the north and south Panamá thrust belts for the origin of the Panamá orocline. Tectonics 9 (2), 261–281.

Stewart, R.H., Stewart, J.L., 1980. Geologic Map of the Panama Canal and Vicinity, Republic of Panama, United States Geological Survey, Miscellaneous Investigations Series Map I-1232.

Stroncik, N.A., Schmincke, G.U., 2002. Palagonite – a review. Int. J. Earth Sci. 91, 680–697.

Vingiani, S., Terribile, F., Meunier, A., Petit, S., 2010. Weathering of basaltic pebbles in a red soil from Sardinia: a microsite approach for the identification of secondary mineral phases. Catena 83, 96–106.